Organ of Corti size is governed by Yap/Tead-mediated progenitor self-renewal

Ksenia Gnedeva[a,b,1], Xizi Wang[a,b], Melissa M. McGovern[c], Matthew Barton[d,2], Litao Tao[a,b], Talon Trecek[a,b], Tanner O. Monroe[e,f], Juan Llamas[a,b], Welly Makmura[a,b], James F. Martin[f,g,h], Andrew K. Groves[c,g,i], Mark Warchol[d], and Neil Segil[a,b,1]

[a]Department of Stem Cell Biology and Regenerative Medicine, Keck Medicine of University of Southern California, Los Angeles, CA 90033; [b]Caruso Department of Otolaryngology–Head and Neck Surgery, Keck Medicine of University of Southern California, Los Angeles, CA 90033; [c]Department of Neuroscience, Baylor College of Medicine, Houston, TX 77030; [d]Department of Otolaryngology, Washington University in St. Louis, St. Louis, MO 63130; [e]Advanced Center for Translational and Genetic Medicine, Lurie Children's Hospital of Chicago, Chicago, IL 60611; [f]Department of Molecular Physiology and Biophysics, Baylor College of Medicine, Houston, TX 77030; [g]Program in Developmental Biology, Baylor College of Medicine, Houston, TX 77030; [h]Cardiomyocyte Renewal Laboratory, Texas Heart Institute, Houston, TX 77030 and [i]Department of Molecular and Human Genetics, Baylor College of Medicine, Houston, TX 77030;

Edited by Marianne E. Bronner, California Institute of Technology, Pasadena, CA, and approved April 21, 2020 (received for review January 6, 2020)

Precise control of organ growth and patterning is executed through a balanced regulation of progenitor self-renewal and differentiation. In the auditory sensory epithelium—the organ of Corti—progenitor cells exit the cell cycle in a coordinated wave between E12.5 and E14.5 before the initiation of sensory receptor cell differentiation, making it a unique system for studying the molecular mechanisms controlling the switch between proliferation and differentiation. Here we identify the Yap/Tead complex as a key regulator of the self-renewal gene network in organ of Corti progenitor cells. We show that Tead transcription factors bind directly to the putative regulatory elements of many stemness- and cell cycle-related genes. We also show that the Tead coactivator protein, Yap, is degraded specifically in the Sox2-positive domain of the cochlear duct, resulting in down-regulation of Tead gene targets. Further, conditional loss of the *Yap* gene in the inner ear results in the formation of significantly smaller auditory and vestibular sensory epithelia, while conditional overexpression of a constitutively active version of *Yap*, *Yap5SA*, is sufficient to prevent cell cycle exit and to prolong sensory tissue growth. We also show that viral gene delivery of *Yap5SA* in the postnatal inner ear sensory epithelia in vivo drives cell cycle reentry after hair cell loss. Taken together, these data highlight the key role of the Yap/Tead transcription factor complex in maintaining inner ear progenitors during development, and suggest new strategies to induce sensory cell regeneration.

Yap | Hippo signaling pathway | organ of Corti | Taz | inner ear

The two major cell types in the sensory organs of the inner ear—hair cells and supporting cells—are derived from the Sox2-positive progenitors specified in the prosensory domain of the otic vesicle (1). In the otolithic vestibular sensory organs, the utricle and the saccule, progenitor cells begin to differentiate into sensory hair cells in the central region of the macula early during embryonic development (2, 3). Concurrent with hair cell differentiation, a wave of cell cycle exit initiates in the macula, spreads toward the periphery of the organ, and gradually restricts progenitor cell proliferation between embryonic day (E) 11.5 and postnatal day (P) 2 (2–6). In contrast to the vestibular sensory epithelia, the auditory organ of Corti undergoes a rapid, 48-h wave of cell cycle exit that arrests progenitor cell proliferation between E12.5 and E14.5, before the initiation of differentiation (2, 7, 8).

Despite these differences in the spatiotemporal patterns of cell cycle exit in the vestibular and auditory sensory epithelia, this exit has been linked to $p27^{Kip1}$ up-regulation in both systems (3, 7, 9). In the organ of Corti, a particularly striking wave of transcriptional activation of the *Cdkn1b* gene, coding for $p27^{Kip1}$, spreads from the apex to the base of the cochlear duct and controls both the timing and the pattern of cell cycle exit (8). However, what initiates this increase in *Cdkn1b* expression remains unclear. In addition, conditional ablation of *Cdkn1b* in the inner ear is not sufficient to completely relieve the block on supporting cell proliferation (9, 10), suggesting the existence of additional repressive mechanisms.

We previously demonstrated that the pattern of cell cycle exit and the dynamics of the vestibular sensory organ growth are controlled by a negative feedback mechanism mediated by the Hippo pathway (6). This evolutionarily conserved signaling cascade controls organ growth mainly by repressing cell proliferation (11). Hippo's downstream effector proteins, Yap and Taz, function in a complex with Tead transcription factors to directly activate the expression of cell cycle, prosurvival, and antiapoptotic genes (12, 13). Mechanistically, the Yap/Tead complex recruits the Mediator complex to distal regulatory elements of their target genes (14, 15). The molecular output of this signaling is highly tissue- and context-dependent, as evidenced,

Significance

While Yap/Tead signaling is well known to influence tissue growth and organ size during development, the molecular outputs of the pathway are tissue- and context-dependent and remain poorly understood. Our work expands the mechanistic understanding of how Yap/Tead signaling controls the precise number of progenitor cells that will be laid down within the developing inner ear to ultimately regulate the final size and function of the sensory organs. We also provide evidence that restoration of hearing and vestibular function may be amenable to YAP-mediated regeneration. Our data show that reactivation of Yap/Tead signaling after hair cell loss induces a proliferative response in vivo—a process thought to be permanently repressed in the mammalian inner ear.

Author contributions: K.G., X.W., M.M.M., M.B., A.K.G., M.W., and N.S. designed research; K.G., X.W., M.M.M., M.B., J.L., and W.M. performed research; L.T., T.T., T.O.M., and J.F.M. contributed new reagents/analytic tools; K.G. and X.W. analyzed data; and K.G., A.K.G., and N.S. wrote the paper.

J.F.M. is a founder and owns shares in Yap therapeutics.

This article is a PNAS Direct Submission.

Data deposition: The data reported in this paper have been deposited in the Gene Expression Omnibus (GEO) database, https://www.ncbi.nlm.nih.gov/geo (accession no. GSE149254).

[1]To whom correspondence may be addressed. Email: gnedeva@usc.edu or nsegil@med.usc.edu.

[2]Deceased January 23, 2017.

This article contains supporting information online at https://www.pnas.org/lookup/suppl/doi:10.1073/pnas.2000175117/-/DCSupplemental.

First published June 1, 2020.

for example, by the large variation observed between Yap/Tead targets in different cancer cell lines (15, 16). However, little is known about the Yap/Tead targetome in developing embryonic tissues in situ, and the role of this transcription factor complex during organ of Corti development has not been investigated.

In this study, we characterized changes in gene expression and chromatin accessibility that occur during cell cycle exit in organ of Corti progenitor cells. We uncovered a key role for the Yap/Tead transcription factor complex in maintaining progenitor cell self-renewal and identified many direct target genes of the Yap/Tead complex in this tissue. In addition, our results suggest that reactivation of Yap/Tead signaling in the postnatal inner ear sensory epithelia is sufficient to induce a proliferative response and so can potentially be used as a strategy to promote inner ear sensory organ regeneration.

Results

A Self-Renewal Gene Network Is Rapidly Repressed in Organ of Corti Progenitor Cells between E12 and E13.5. To identify the gene network that controls self-renewal in the developing organ of Corti, we analyzed gene expression in actively dividing (E12.0) and postmitotic (E13.5) progenitor cells. We used *Sox2-GFP* mice (17) to purify progenitors at E12.0 and *p27^{Kip}-GFP* mice (8) to purify progenitor cells at E13.5 (Fig. 1*A*). Principal component analysis of RNA sequencing (RNA-seq) data revealed that the overwhelming percentage of variance (96%) between E12.0 and E13.5 samples could be explained by the first principal component, composed of genes associated with cell division (Fig. 1 *B* and *C* and Dataset S1). In particular, 365 genes shown to be associated with regulation of the cell cycle (GO:0051726) were significantly differentially expressed between the two time points, facilitating a sharp transition to a postmitotic state (false discovery rate [FDR] <0.01) (Fig. 1*D*). These genes included known key regulators of cell proliferation in the developing cochlea, such as cyclin D1 (*Ccnd1*) (10) and p27^{Kip1} (*Cdkn1b*) (7, 9).

Tead Transcription Factors Control the Self-Renewal Gene Network in the Organ of Corti Progenitor Cells. To gain a mechanistic understanding of how proliferation in the cochlear prosensory domain is controlled before cell cycle exit, we identified the presumptive regulatory elements specific for the self-renewal state. By profiling chromatin accessibility in E12.0 and E13.5 organ of Corti progenitor cells using ATAC sequencing (ATAC-seq), we demonstrated that more than two-thirds of all accessible chromatin regions identified in E12.0 progenitor cells remained open as these cells exited the cell cycle, while one-third of the regions were specifically associated with the self-renewal state (Fig. 1*E*). Transcription factor motif enrichment analysis, using Homer software (18), demonstrated that Tead DNA-binding motifs were among the most significantly enriched in accessible chromatin regions specific to E12.0 progenitors and regions common to E12.0 and E13.5 progenitors, but not in accessible chromatin regions seen only in E13.5 progenitors (Fig. 1 *F* and *F′*).

Using a recently published low-input in situ alternative to chromatin immunoprecipitation (ChIP) sequencing, CUT&RUN (19, 20), we tested whether Tead transcription factors bound directly to the regulatory elements associated with the proliferative state in the E12.0 organ of Corti. Our analysis identified 74,966 chromatin regions occupied by Tead inclusive of two CUT&RUN replicates, almost 40% of which (28,648) mapped to the open chromatin regions identified by ATAC-seq at the same stage (Fig. 2*A*). We also performed CUT&RUN for histone 3 lysine 27 acetylation (H3K27Ac), a known marker of active promoters and enhancers (21, 22). Strikingly, >85% (24,845) of Tead-bound accessible chromatin regions were also marked by H3K27Ac, suggesting that these regions are active regulatory elements in E12.0 progenitor cells. GREAT analysis (23) revealed that terms associated with stem cell maintenance and cell division were among the most enriched in the genes closest to, and thus likely to be controlled by (22, 24), Tead-bound putative regulatory elements (Fig. 2*C*).

Chromatin accessibility and H3K27Ac status of most (>85%) putative regulatory elements bound by Tead in E12.0 progenitors remained unchanged as these cells exited the cell cycle (Fig. 2 *D* and *E*). Nevertheless, the putative Tead targets included many positive regulators of the cell cycle that were down-regulated between E12.0 and E13.5 (Fig. 2*F*). Examples of such regulators include ATP-dependent RNA helicase (*Ddx3x*) (25), Aurora B kinase (*Aurkb*) (26), Cyclin d1 (*Ccnd1*) (27), and mitotic centromere-associated kinase (*Kif2c*) (28), among many others (Fig. 2*E* and Dataset S2). Gene Set Enrichment Analysis (GSEA) (29) confirmed that putative Tead target genes associated with the cell cycle (GO:0007049) included almost none of the negative regulators and thus were significantly coordinately down-regulated in the cochlear progenitors between E12.0 and E13.5 (Fig. 2*G*). These data strongly suggest that Tead transcription factors directly control the self-renewal gene network in the developing organ of Corti before the cell cycle exit.

Degradation of Yap Protein Is Associated with Cell Cycle Exit in the Organ of Corti. It is well established that Tead transcription factors activate gene expression in a complex with Yap and Taz cofactors, the downstream effectors of the Hippo signaling pathway (12) (Fig. 3*B*). Gene Ontology (GO) analysis identified Hippo signaling as one of the most enriched terms among the genes differentially expressed between E12.0 and E13.5 (Fig. 1*C*). In 22 of 30 genes currently associated with Hippo signaling (GO:0035329), expression was significantly changed in sensory progenitor cells during cell cycle exit (FDR <0.01; Fig. 3*A*). Most notably, between E12.0 and E13.5, the transcriptional activators *Yap* and *Wwtr1* (*Taz*) were down-regulated by more than twofold, and *Dlg5*, a known suppressor of the Hippo signaling pathway that inhibits the association between Mst1/2 and Lats1/2 kinases (30), was down-regulated by more than fivefold. In addition, *Mst2*, *Lats1*, *Nf2*, *Vgll4*, and *Wwc1*(*Kibra*) were all significantly up-regulated in postmitotic progenitor cells, consistent with activation of Hippo signaling (31).

Because the level of gene expression does not directly correlate with Yap activity, we investigated the phosphorylation state of the key proteins in the Hippo pathway in the actively dividing and postmitotic organ of Corti. The wave of cell cycle exit initiated at the apex at E12.5 reaches the base of the cochlea by E14.5; thus, these two time points were chosen for the analysis (7). We demonstrated that although the total amount of Yap protein remained relatively unchanged between E12.5 and E14.5, the level of Yap phosphorylation increased between these stages, suggesting activation of Hippo signaling at E14.5 (Fig. 3*C*).

In addition to phosphorylation status, nuclear versus cytoplasmic localization of Yap serves as a proxy for its activity (31) (Fig. 3*B*); thus, we focused on Yap protein distribution during normal organ of Corti development. At E12.5, when the first progenitor cells at the apex of the prosensory domain of the cochlear duct begin to exit the cell cycle, cytoplasmic retention and some degradation of Yap protein are observed (Fig. 3*D*). As the wave of cell cycle exit progresses and reaches the base of the cochlea by E14.5, the Sox2-positive domain, in which the first Atoh1-positive sensory cell differentiation occurs, can be clearly identified as a Yap protein-depleted region in which little to no nuclear Yap protein can be observed (Fig. 3*D*). This depletion becomes even more striking at P6, when regenerative potential is permanently lost from the cochlear sensory epithelia (32).

Conditional Loss of *Yap* in the Inner Ear Results in Formation of Significantly Smaller Sensory Organs. To directly test the role of the Yap/Tead complex in driving progenitor cell proliferation, we generated conditional knockout mice deficient for *Yap* in the

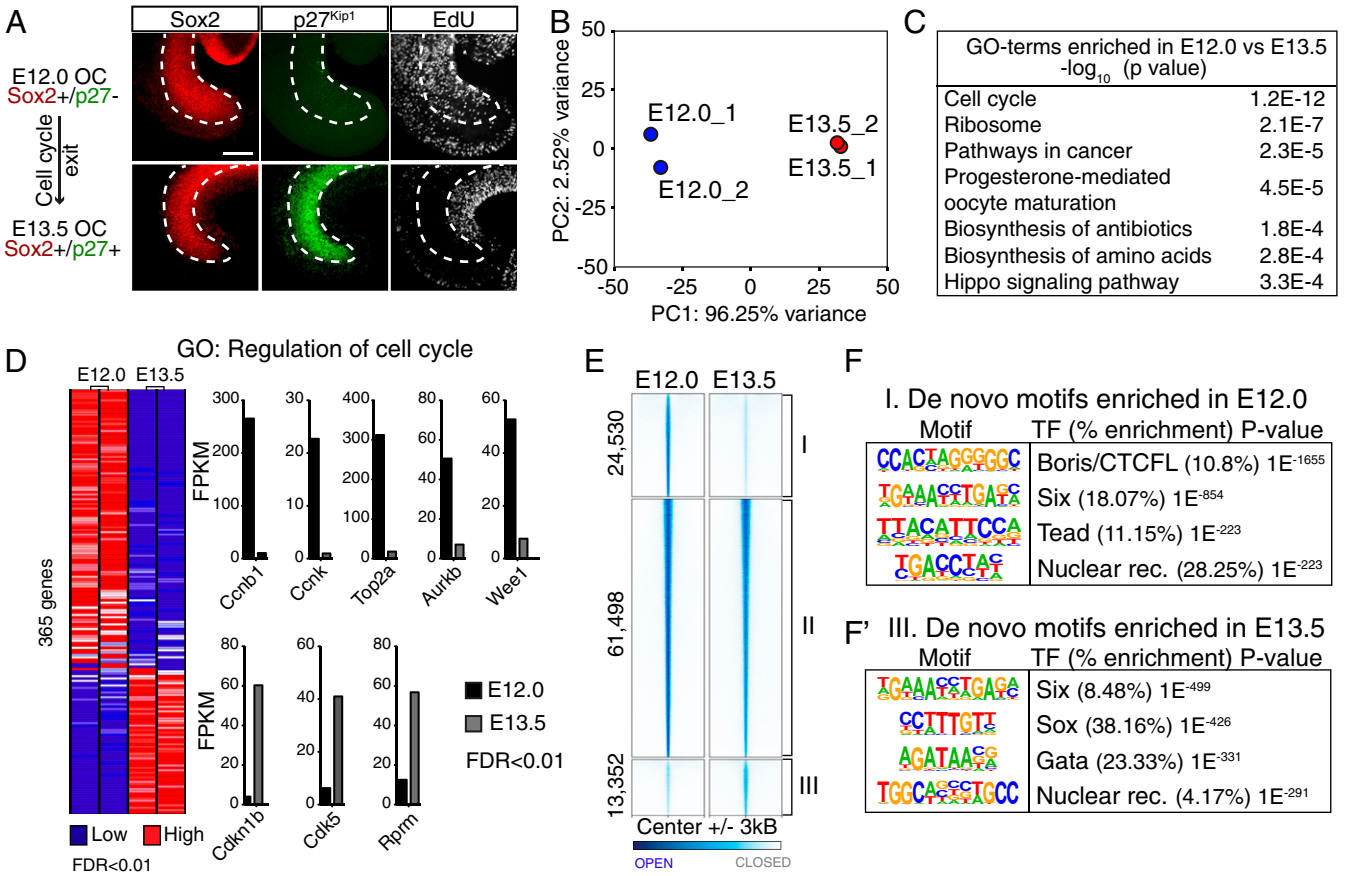

Fig. 1. RNA-seq and ATAC-seq reveal dramatic changes in the regulation of self-renewal genes in organ of Corti progenitor cells between E12.0 and E13.5. (*A*) To demonstrate the timing of cell cycle exit in the organ of Corti, an EdU pulse was applied 30 min before inner ear dissections at E12.0 and E13.5. Immunofluorescence analysis shows that at E12.0 Sox2-positive progenitors incorporate EdU, confirming that these are actively cycling cells (*Top*). In contrast, at E13.5, the Sox2-positive progenitor cells up-regulate $p27^{Kip1}$ expression and no longer incorporate EdU (*Bottom*). To FACS-purify organ of Corti progenitor cells before (E12.0) and after (E13.5) the cell cycle exit, *Sox2-GFP* and *$p27^{Kip}$-GFP* mice were used. (Scale bars: 100 μm.) (*B*) Principal component analysis of RNA-seq data from E12.0 and E13.5 organ of Corti progenitor cells demonstrating that the two replicates collected for each stage cluster tightly with each other. Almost all the variance between E12.0 and E13.5 samples can be explained by the first principal component (PC1 = 96.25%). (*C*) GO enrichment analysis performed with DAVID software demonstrating that the term associated with the cell cycle is most enriched in the genes differentially expressed (FDR <0.01) between E12.0 and E13.5 in the organ of Corti. (*D*, *Left*) Heatmap demonstrating the relative expression levels of 365 cell cycle genes differentially expressed between E12.0 and E13.5 progenitor cells (FDR <0.01; $n = 2$ for each condition). Highly expressed genes are shown in red, while the genes with relatively low levels of expression are depicted in blue. (*D*, *Right*) Bar graphs showing FPKM values of the top up-regulated and down-regulated genes. (*E*) Heatmap showing differentially accessible chromatin regions determined by ATAC-seq in E12.0 and E13.5 organ of Corti progenitor cells, generated using deepTools. The open chromatin regions, specific to E12.0 (24,530), common between E12.0 and E13.5 (61,498), and specific to E13.5 (13,352) are identified. (*F*) The top-four transcription factor DNA-binding motifs enriched in the open chromatin regions preferentially accessible at E12.0 and at E13.5 (*F'*) in the organ of Corti progenitor cells identified using Homer motif enrichment analysis. The Tead DNA-binding motif is significantly enriched in E12.0-specific regions.

sensory organs of the inner ear using *Pax2-Cre* and $Yap^{fl/fl}$ mice (33, 34). Consistent with previous reports (7, 8), at E12.5 an average of 70% of the Sox2-positive sensory progenitor cells in the midbase of the cochlear duct were actively cycling in Cre-negative, phenotypically wild-type (WT) littermates (Fig. 4 *A* and *B*). The percentage of mitotic cells in the Sox2-positive domain decreased by >20% in conditional *Yap* knockouts ($P < 0.01$; $n = 9$). This decrease in cell proliferation was accompanied by a significant reduction in the total number of Sox2-positive cells ($P < 0.05$; $n = 9$) (*SI Appendix*, Fig. S1 *A* and *B*); however, we did not observe apoptotic cells within the cochlear duct of either WT or Yap CKO littermates, as shown by the absence of active caspase 3 labeling ($n = 6$) (*SI Appendix*, Fig. S1*A*).

We confirmed the efficiency of *Pax2-Cre*–driven recombination by demonstrating an absence of the Yap protein in *Yap* CKO cochleae at E13.5 (*SI Appendix*, Fig. S1*C*). We noted that at this stage, $p27^{Kip1}$ expression expanded to the abneural domain in the apex of the cochlear duct, where no EdU incorporation was observed in the knockouts (*SI Appendix*, Fig. S1 *C* and *D*). Nevertheless, up-regulation of $p27^{Kip1}$ and cell cycle exit in the prosensory domain still occurred in a wave spreading from apex to base in the *Yap* mutants, suggesting no direct correlation between loss of *Yap* and transcriptional *Cdkn1b* up-regulation.

Consistent with the reported pattern of *Pax2-Cre* expression (33), by later stages of embryonic development, *Yap* CKO animals exhibited midbrain/hindbrain defects and died shortly after birth (*SI Appendix*, Fig. S2*A*). At E18.5, decreased numbers of the sensory progenitors in conditional *Yap* mutants manifested in a drastic reduction in the size of the organ of Corti (Fig. 4 *C* and *F*). However, the pattern of cellular differentiation remained largely intact, with four rows of hair cells and underlying rows of supporting cells detected throughout the entire length of the cochlear duct (Fig. 4 *C* and *D*). Although the overall number of hair cells was reduced proportionally to the reduction in cochlear length (Fig. 4*G*), we consistently observed ectopic hair cells and supporting cells on the abneural side of the cochlear duct at the

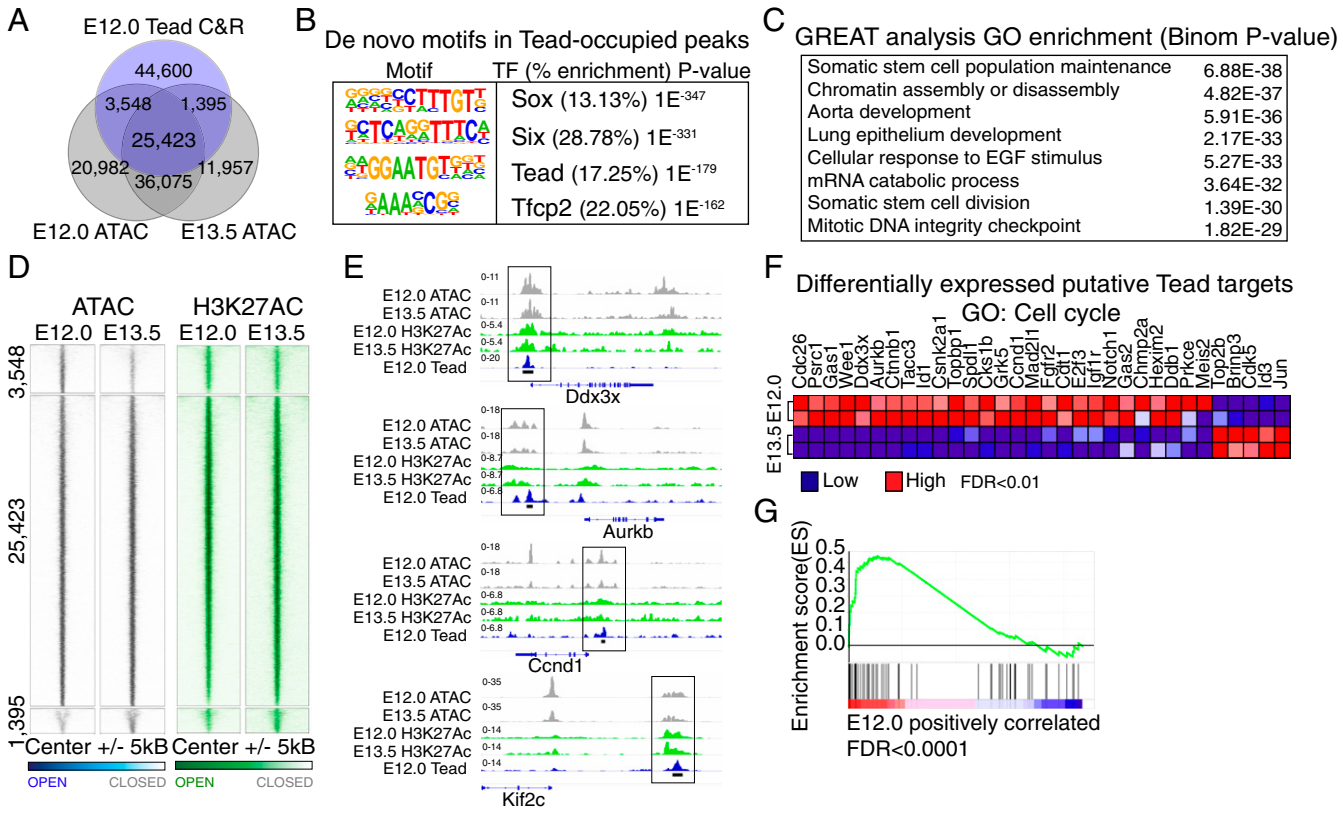

Fig. 2. Tead transcription factors directly bound to the putative regulatory elements of many stemness and cell cycle genes. (*A*) Venn diagram demonstrating the overlaps among E12.0 Tead-bound, E12.0-accessible (E12.0 ATAC), and E13.5-accessible (E13.5 ATAC) chromatin regions. A clear majority (25,423) of the Tead-bound chromatin regions identified by CUT&RUN (C&R) at E12.0 were also identified through ATAC-seq as being accessible at that stage and remained accessible at E13.5, when the progenitor cells exit the cell cycle. (*B*) Homer motif enrichment analysis confirming that a Tead DNA-binding motif is enriched in the Tead-bound chromatin regions that are accessible at E12.0. (*C*) Identified using GREAT software, GO terms associated with stem cell maintenance and cell division are enriched in the genes associated with the Tead-bound and ATAC-accessible chromatin regions at E12.0. (*D*) deepTools-generated heatmaps showing a comparative analysis of the chromatin accessibility, assessed by ATAC-seq (gray), and H3K27Ac (green) of the chromatin regions occupied by Tead in E12.0 progenitor cells. As also demonstrated by the Venn diagram in *A*, >85% (25,423) of Tead-occupied accessible chromatin regions identified at E12.0 remain accessible after the cell cycle exit at E13.5. The H3K27Ac status of the same regions remains largely unchanged. (*E*) bigWig tracks for the representative examples of the putative Tead target genes associated with cell cycle progression visualized using the IGV. Note that chromatin associability (ATAC; gray) and H3K27Ac (green) is unchanged at the putative regulatory elements occupied by Tead (blue; black bars). (*F*) Heatmap showing relative expression levels of the differentially expressed putative Tead targets associated with cell cycle (FDR < 0.01; $n = 2$ for each condition). Highly expressed genes are shown in red, while the genes with relatively low levels of expression are depicted in blue. (*G*) GSEA enrichment plot demonstrating a significant correlation (FDR <0.0001) between gene expression and Tead-occupancy for the cell cycle-related genes (GO:0007049) at E12.0.

apex, where expanded $p27^{Kip1}$ expression was detected at E13.5 (Fig. 4 *C–E*). Confirming our previous observation that Yap controls growth of the vestibular organs (6), the utricle and saccule were also significantly smaller in *Yap* CKO mice (*SI Appendix*, Fig. S2 *B–D*). Nevertheless, the hair cell density remained unchanged in these organs (*SI Appendix*, Fig. S2*E*).

Collectively, these observations strongly suggest that while $p27^{Kip1}$ up-regulation serves as the major driver of cell cycle exit in the prosensory domain of the cochlear duct, Yap signaling controls the number of progenitor cells to be formed in the auditory and vestibular sensory organs to regulate their final size.

Constitutive Activation of Yap Prevents Cell Cycle Exit Resulting in Sensory Epithelia Overgrowth. If loss of the Yap/Tead transcription complex causes cell cycle exit in the sensory epithelia of the inner ear, then preventing Yap degradation should result in prolonged cell proliferation. To test this hypothesis, we used a transgenic mouse model in which a constitutively active version of Yap, Yap5SA, can be expressed conditionally on Cre-driven recombination (35). *Sox2-CreER* (17) mice were used to induce the expression of FLAG-tagged Yap5SA in the sensory progenitor cells before the initiation of cell cycle exit at E11.5 (Fig. 5*A* and *SI Appendix*, Fig. S3 *A* and *B*). The progression of cell cycle exit in the sensory organs was evaluated by assessing Ki67 positivity at E14.5 and E17.5, 3 and 6 d after the induction, respectively. The samples were counterstained with antibodies against Sox2 and FLAG to identify the cells in which Yap5SA expression was induced. However, no FLAG labeling was observed in these samples, suggesting rapid Yap5SA-FLAG degradation, loss of the cells in which recombination was induced, or, most likely, failure to induce the overexpression construct in organ of Corti progenitors. As a result, no excess Ki67 and Sox2 double-positive cells were found in the induced organs of Corti at E14.5 compared with Cre-negative controls (*SI Appendix*, Fig. S3*C*).

In contrast to the organ of Corti, robust induction of Yap5SA-FLAG expression was observed in the vestibular sensory epithelia at E14.5, 3 d after Cre induction (Fig. 5*D*). The same organs showed a greater than twofold increase in the number of Ki67 and Sox2 double-positive cells in the utricular macula, where cell cycle exit was already evident in the Cre-negative control littermates (Fig. 5 *B* and *D*). This overproliferation phenotype became more overt at E17.5, when the vestibular organs of Yap5SA-induced animals appeared grossly overgrown,

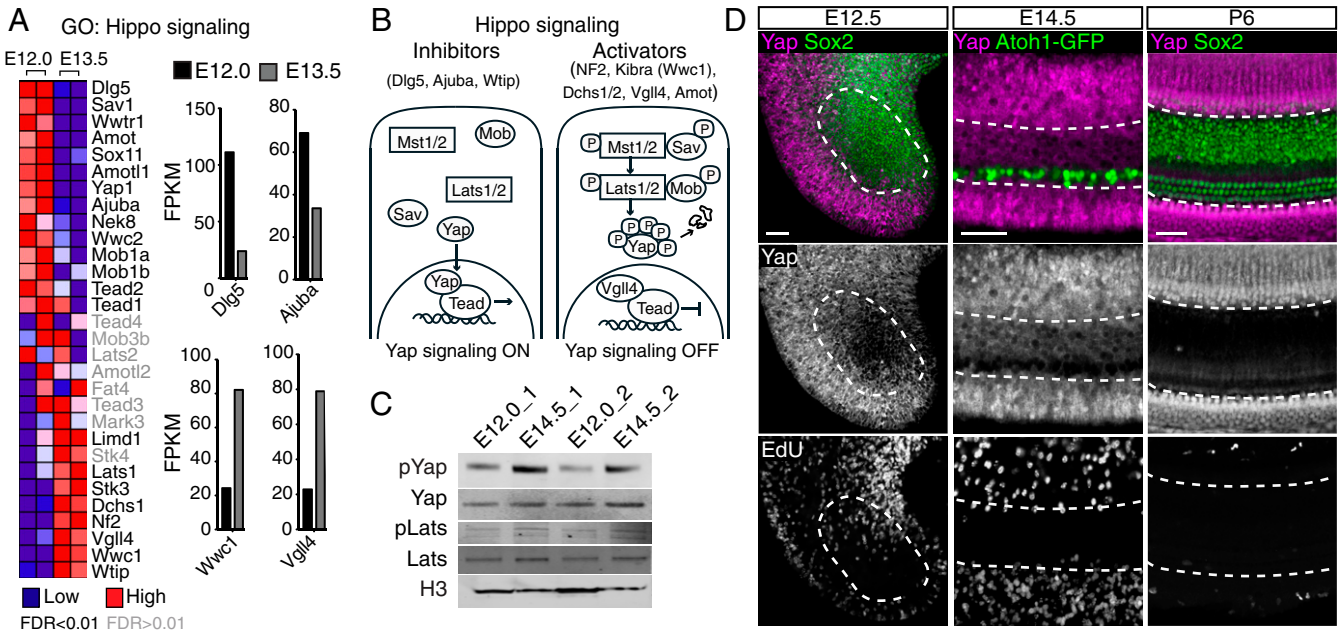

Fig. 3. Hippo signaling activation and degradation of Yap protein coincide with the wave of cell cycle exit in the developing organ of Corti. (*A*, *Left*) Heatmap showing relative expression levels of 30 genes associated with the Hippo pathway in E12.0 and E13.5 organ of Corti progenitor cells. Highly expressed genes are shown in red, while genes with relatively low levels of expression are depicted in blue. Differentially expressed genes are highlighted in black (FDR <0.01; $n = 2$ for each condition). (*A*, *Right*) Bar graphs showing FPKM values of some of these up-regulated and down-regulated genes. (*B*) Schematic depiction of the Hippo pathway. When Hippo signaling is inactive, Yap transcriptional cofactor may translocate to the nucleus, where, together with Tead transcription factors, it activates gene expression. Phosphorylation and activation of Mst1/2 and Lats1/2 kinases in the Hippo pathway result in phosphorylation and cytoplasmic retention of Yap, where it is targeted for degradation. Note that most inhibitors of the Hippo pathway (positive regulators of Yap signaling) are highly expressed at E12.0, while most Hippo activators (negative regulators of Yap signaling) are up-regulated at E13.5. (*C*) Western blot analysis of epithelial cochlear duct lysates comparing Hippo signaling activity at E12.0 and E14.5. Consistent with Hippo signaling activation at E14.5, although the overall levels of Yap protein are unchanged, the levels of the inactive, phosphorylated form of Yap are increased at this stage ($n = 3$ for each condition). (*D*) To demonstrate the timing of Yap protein degradation compared with the cell cycle exit in the organ of Corti, an EdU pulse was delivered 30 min before euthanizing the pregnant dams at E12.5 or E14.5 and neonatal pups at P6. Immunofluorescence analysis shows progressive depletion of Yap protein (purple, white) in the Sox2-positive (green and outlined) domain of the cochlear duct as it becomes devoid of EdU-positive (white) proliferating progenitor cells in E12.5 (*Left*; $n = 4$), E14.5 (*Middle*; $n = 4$), and P6 (*Right*; $n = 6$). (Scale bars: 50 μm.)

with Sox2-positive cells continuing to proliferate throughout the macula (Fig. 5 *C* and *E*). This increase in cell proliferation impaired differentiation or survival of the sensory receptors, as the number of Myo7A-positive hair cells remained relatively low in the Yap5SA-expressing tissue compared with controls (Fig. 5 *C* and *E*).

Constitutive Activation of Yap via Intraventricular Brain Viral Injection Triggers Cell Cycle Reentry in the Postnatal Sensory Epithelia of the Inner Ear. Induction of the Yap5SA transgene becomes further restricted to just hair cells in the inner ear sensory organs at later embryonic ages (*SI Appendix*, Fig. S4*C*). Therefore, to analyze the function of Yap/Tead complex in vivo postnatally, we used viral vectors for gene delivery into the inner ear. Round window, posterior semicircular canal, and intraventricular injections are currently used to achieve gene transfer into hair cells and supporting cells. These procedures require invasive surgery and are labor-intensive, time-consuming, and low-throughput. Because inner ear perilymph is connected directly to the cerebrospinal fluid via the cochlear aqueduct (*SI Appendix*, Fig. S5*A*) (36), we tested whether virus injected intraventricularly would spread into the inner ear in neonatal mice. In brief, 5 μL of the Anc80-GFP virus (37) was injected freehand into the lateral ventricle of P1 to P6 neonatal mice anesthetized on ice (38). Using this new method, we achieved efficient gene delivery into the central nervous system and both vestibular and auditory sensory epithelia (*SI Appendix*, Fig. S4*B*). The Anc80 vector has been previously shown to predominantly infect hair cells, while supporting cells remain uninfected (37). Importantly, we also demonstrated that intraventricular gene delivery in *Pou4f3*$^{DTR/+}$ mice (39), in which hair cells were killed by diphtheria toxin injection 1 d earlier, resulted in effective gene transfer in the residual supporting cells (*SI Appendix*, Fig. S5 *C* and *D*).

Using this new viral delivery method, we tested the effects of Yap signaling activation in the inner ear sensory epithelia after hair cell ablation (Fig. 6*A*). Diphtheria toxin was administered at P6, the stage at which spontaneous regeneration is no longer observed in the organ of Corti in vivo (32). The next day, Anc80-GFP control or Anc80-Yap5SA-GFP virus was administered intraventricularly to the animals carrying the *DTR* allele. The animals were injected with EdU and euthanized at 3 d after viral injections. We found that *Yap5SA* expression resulted in robust supporting cell cycle reentry in the utricular macula, where numerous Sox2- and EdU-positive supporting cells were observed (Fig. 6 *B* and *C*). Cell cycle reentry was also initiated upon Yap5SA overexpression in Sox2-positive cells in Kölliker's organ and in the organ of Corti, albeit at a lower efficiency (Fig. 6 *B′* and *D*). These data demonstrate that activation of Yap signaling is sufficient to drive supporting cell proliferation in postnatal inner ear sensory organs—a process normally blocked in mammals, but necessary for sensory hair cell regeneration in nonmammalian vertebrates.

Discussion

In this study, we characterize the role of the Yap/Tead complex in maintaining the proliferative state of organ of Corti progenitors before establishment of the postmitotic prosensory domain.

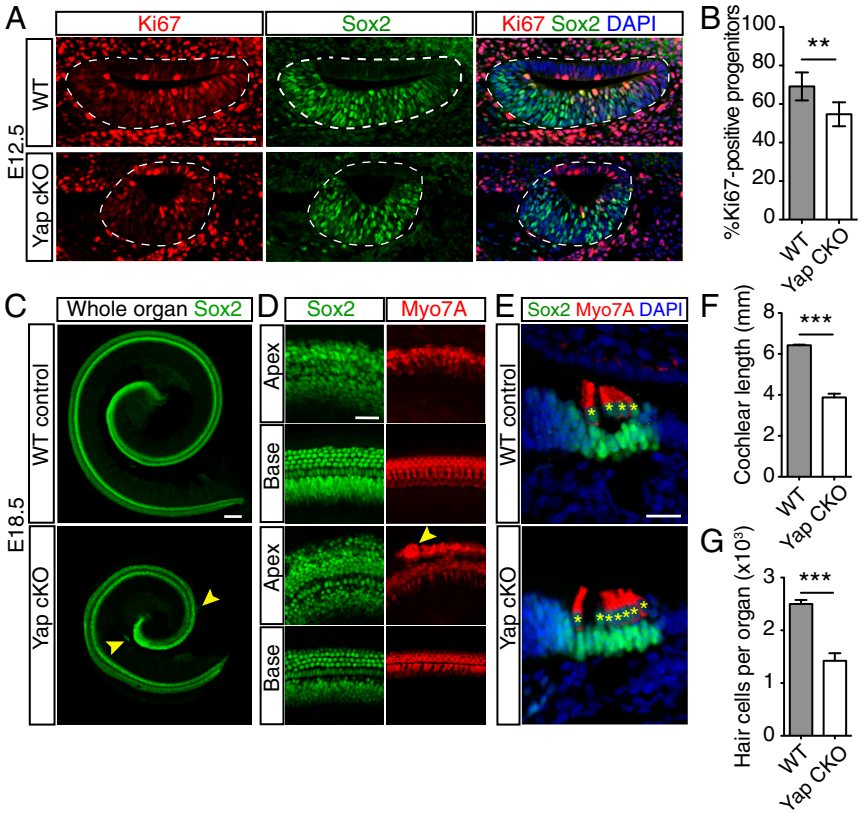

Fig. 4. Conditional loss of Yap in the inner ear results in the formation of significantly smaller sensory organs. (*A*) Immunofluorescence analysis showing a reduction in number of Ki67-positive (red) cells in the Sox2-positive (green) prosensory domain of the cochlear ducts (outlined) of the Yap CKO (*Pax2-Cre*$^{Cre/+}$ *Yap*$^{fl/fl}$) embryos compared with the WT (*Pax2-Cre*$^{+/+}$ *Yap*$^{fl/fl}$) littermates at E12.5 ($n = 9$ for each condition). Nuclei are counterstained with DAPI (blue). (Scale bars: 100 μm.) (*B*) Bar graph showing a significant decrease in the proportion of mitotically active Sox2-positive cells in Yap CKO cochlear ducts compared with WT controls ($n = 9$ for each condition; $P = 0.0049$). (*C*) Representative immunofluorescence images of the whole-mount cochlear ducts of the WT and Yap CKO littermate embryos at E18.5 labeled for Sox2 (green) to visualize the organ of Corti ($n = 4$ for each condition). MosaicJ, an ImageJ plugin, was used to assemble a whole mount mosaic from the individual image. (*D*) The apical and basal turns of WT and Yap CKO cochlea. Supporting cells are labeled for Sox2 (green), and hair cells are labeled for Myo7A (red). Ectopic hair cells and supporting cells are seen on the abneural side of the organ of Corti in Yap CKO (arrowhead). (Scale bars: 100 μm.) (*E*) Immunofluorescence images of the sections through the apical turn of the cochlear ducts of the WT and Yap CKO littermate embryos at E18.5. Supporting cells are labeled for Sox2 (green), and hair cells are labeled for Myo7A (red). Ectopic hair cells are seen in Yap CKO (asterisks). Nuclei are counterstained with DAPI (blue). (Scale bars: 50 μm.) (*F*) Bar graph showing a significant decrease in Yap CKO cochlear duct size at E18.5 compared with WT littermates ($n = 4$ for each condition; $P < 0.0001$). (*G*) Bar graph showing a significant decrease in the number of hair cells in the Yap CKO cochlear ducts compared with WT littermates ($n = 4$ for each condition; $P = 0.0006$).

We demonstrate that Tead transcription factors directly control expression of cell cycle genes, and that reactivation of Yap/Tead signaling is sufficient to prevent cell cycle exit during embryogenesis and to induce supporting cell proliferation postnatally.

Before our present work, most research was focused on Wnt signaling as a major regulator of progenitor self-renewal in the sensory epithelia of the inner ear (40). Similar to Yap signaling, canonical Wnt activity is detected at high levels in the prosensory domain of the cochlear duct before p27^{Kip1} up-regulation, and is reduced thereafter (41). In addition, both genetic and small-molecule activation of Wnt signaling are sufficient to promote cell proliferation in the embryonic and neonatal organ of Corti (41–44). Although we show that loss of Yap results in significant reduction in the proportion of dividing cells within the Sox2-positive prosensory domain of the cochlear duct at E12.5, the progenitor cells do not completely lose their mitotic capacity in the absence of Yap/Tead signaling. Therefore, it is likely that other mitogenic pathways, such as Wnt, act in parallel with Yap/Tead signaling to maintain the self-renewal state in the cochlear prosensory cells. It is important to note, however, that Taz, a closely related homolog of Yap, is also expressed in the sensory progenitors of the cochlea duct (Fig. 3*A*). Taz can drive cell proliferation in complex with Tead transcription factors (12, 13), and thus may partially compensate for the loss of Yap in conditional inner ear knockouts. Interestingly, a recent study demonstrated that conditional inactivation of *Ctnnb1* (β-catenin), as early as E10.5, does not result in a significant reduction in the length of the organ of Corti or in the numbers of supporting and hair cells, suggesting normal progenitor cell proliferation in the absence of canonical Wnt signaling (45). In stark contrast, conditional loss of Yap drastically affects the size of the organ of Corti, suggesting the dominance of Yap/Taz/Tead signaling in driving cell proliferation during development.

Given the similar patterns of Yap degradation and p27^{Kip1} up-regulation in the cochlea, it is attractive to propose a functional relationship between the pathways, or to hypothesize that the stability of both proteins is regulated by the same upstream mechanisms. Recent work indicates that YAP can be poly-ubiquitinated by the SCF-SKP2 E3 ligase complex, which enhances its nuclear translocation and Yap/Tead complex stability (46). The SCF-SKP2 complex is a well-established regulator of the protein levels of cyclins and cyclin-dependent kinase inhibitors and can degrade p27^{Kip1} (47). Consistent with this observation, our data demonstrate an almost fourfold decrease in

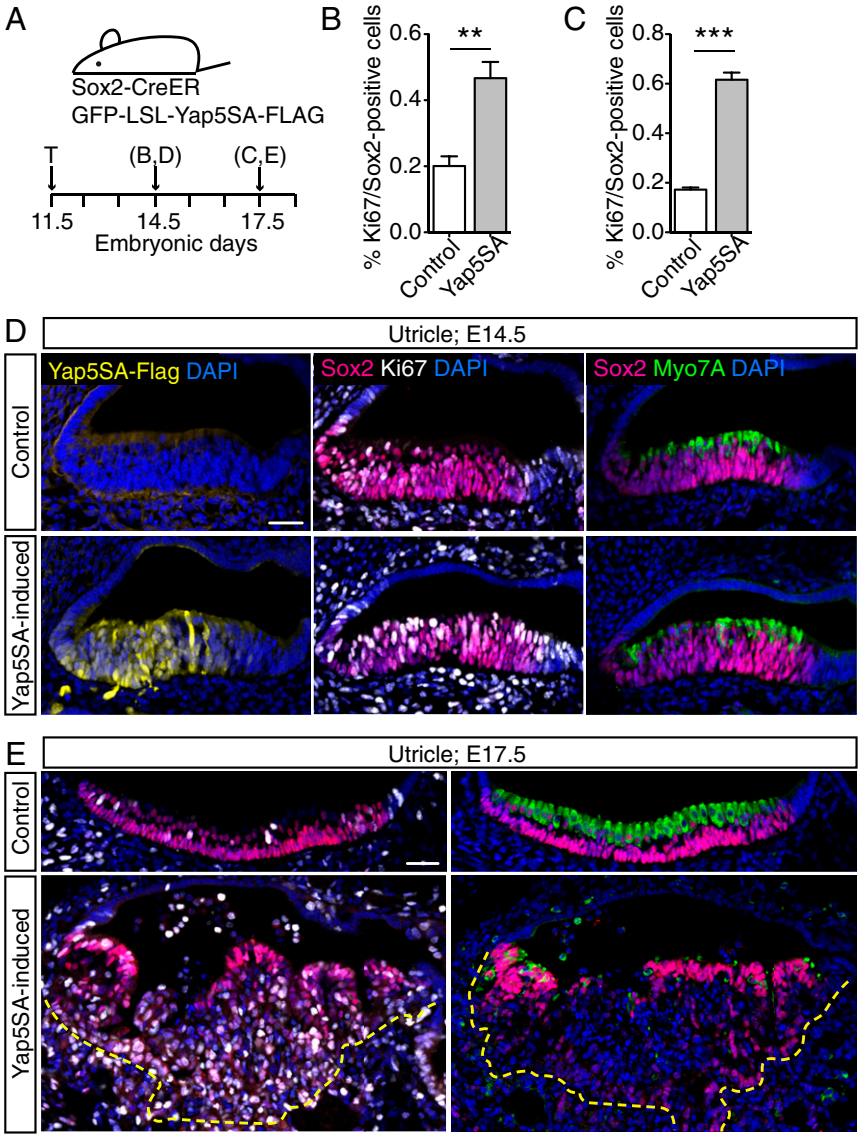

Fig. 5. Conditional constitutive activation of Yap in the inner ear sensory progenitor cells results in excessive proliferation and overgrowth. (*A*) Schematic representation of the experimental design for conditional activation of *Yap5SA* expression in the sensory epithelia of the inner ear. Tamoxifen (T) was administered at E11.5, and analysis of WT control (*Sox2-CreER*$^{+/+}$ *GFP-LSL-Yap5SA-FLAG*) and Yap5SA-induced (*Sox2-CreER*$^{Cre/+}$ *GFP-LSL-Yap5SA-FLAG*) littermates was performed at E14.5 or E17.5. (*B*) A significant increase in the percentage of Ki67- and Sox2-positive proliferating progenitor cells is observed in the utricles where *Yap5SA* expression was induced compared with the WT littermate controls ($n = 4$ for each condition; $P = 0.0036$). (*C*) Significantly increased progenitor cell proliferation, quantified as percentage of Ki67- and Sox2-positive cells, is also observed at E17.5 in the Yap5SA-induced utricles ($n = 3$ for each condition; $P < 0.0001$). (*D*) Immunofluorescence analysis of sections of the inner ears of the WT and Yap5SA-induced littermate embryos at E14.5 demonstrating that cell proliferation (Ki67; white) is markedly increased but hair cell differentiation (Myo7A; green) is unchanged in the Sox2-positive (red) progenitor cells in the utricular macula. The cells in which Yap5SA-FLAG induction is achieved are shown in yellow. Nuclei of all cells are counterstained with DAPI (blue). (Scale bars: 50 μm.) (*E*) The same analysis as in *D* performed at E17.5 demonstrating a dramatic increase in cell proliferation (Ki67; white) within the Sox2-positive (red) utricular macula, with reduced hair cell differentiation (Myo7A; green). Nuclei are counterstained with DAPI (blue). (Scale bars: 50 μm.)

Skp2 expression in postmitotic organ of Corti progenitor cells (Dataset S1). Moreover, the Yap/Tead complex was recently shown to directly regulate *Skp2* transcription in human breast cancers, where high Yap and low $p21^{Cip1}$/$p27^{Kip1}$ expression levels are correlated (48). Our data support these observations, as we identify the *Skp2* gene as one of the direct Tead targets in the sensory epithelia using the CUT&RUN assay (Dataset S2) and show that conditional loss of Yap in the inner ear results in an expansion of $p27^{Kip1}$ expression in the apex of the cochlear duct.

Our data do not support the idea that Yap/Tead degradation initiates the apical-to-basal wave of transcriptional $p27^{Kip1}$ activation, a form of cell cycle control unique to the organ of Corti (8). It does, however, suggest a similar transcriptional level of control for the Yap/Tead pathway in the developing organ of Corti. In particular, we show that Yap expression is down-regulated, while expression of the core Hippo kinases and adaptor proteins is up-regulated, as progenitor cells transition into a postmitotic state (Dataset S1). More research is needed to understand the intertwined, yet distinct roles for Yap and $p27^{Kip1}$ as upstream regulators of the cell cycle in the inner ear.

In addition to expanding the mechanistic understanding of early inner ear sensory epithelia development, our work provides insight into how regenerative responses can be initiated in the inner ear sensory tissue. Adult mammalian supporting cells in

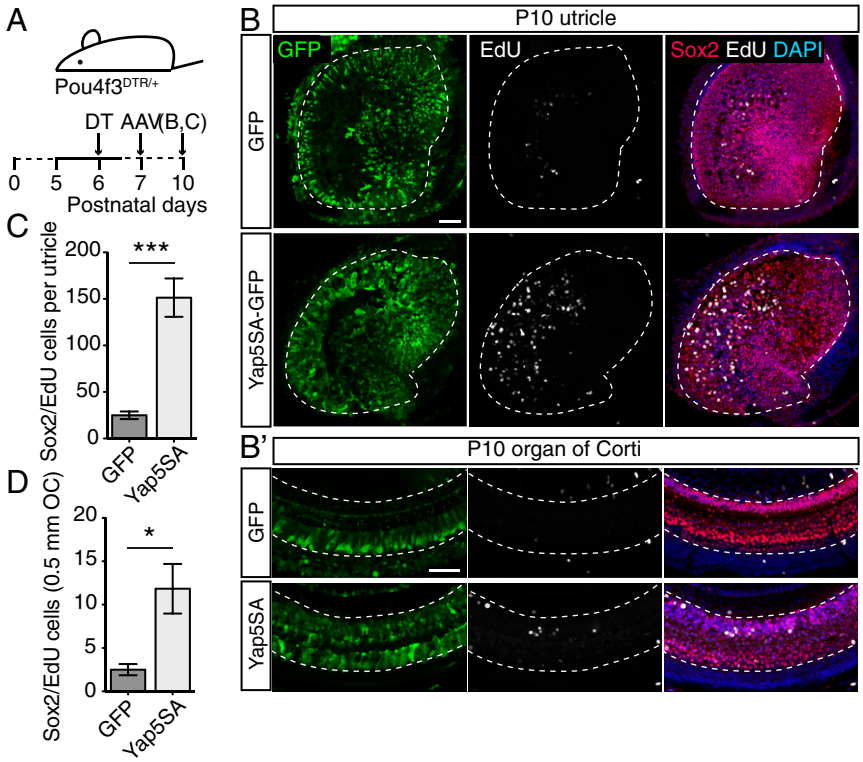

Fig. 6. Viral overexpression of Yap5SA in the postnatal inner ear sensory organs in vivo initiates cell cycle reentry. (*A*) Schematic representation of the experimental design for diphtheria toxin (DT) hair cell ablation and the subsequent adeno-associated virus (AAV) administration and analysis of neonatal *Pou4f3*$^{DTR/+}$ mice. (*B*) Immunofluorescence analysis of P10 whole-mount utricles isolated from the *Pou4f3*$^{DTR/+}$ mice in which hair cell ablation was induced at P6 and GFP-control or Yap5SA-GFP AAV injections were performed at P7. To identify the cells that have reentered the cell cycle, an EdU pulse was administered at P10, 30 min before euthanizing the animals. Yap5SA overexpression results in a marked increase in cell proliferation (EdU; white) of Sox2-positive (red) supporting cells in the utricular macula. (*B'*) The same analysis as in *B* for the organ of Corti. (*C*) The increase in the number of proliferating Sox2-positive supporting cells in the utricles isolated from the Yap5SA-infected mice compared with the GFP-infected controls is statistically significant ($n = 4$ for each condition; $P = 0.0009$). (*D*) The increase in the numbers of proliferating Sox2-positive cells in the cochlea isolated from the Yap5SA-infected mice compared with the GFP-infected controls is statistically significant ($n = 6$ for each condition; $P = 0.032$). Nuclei are counterstained with DAPI (blue). (Scale bars: 100 μm.)

both vestibular and auditory epithelia lack the capacity to reenter the cell cycle to regenerate lost hair cells in vivo—the main mechanism by which hearing and vestibular functions are restored in birds (49–52). Despite considerable effort, there has been only limited success in inducing such proliferative responses in postnatal mammalian sensory organs in vivo, mostly via constitutive activation of Wnt signaling (42–44). Recent research clearly demonstrates that the Hippo pathway antagonizes Wnt to control tissue growth and regeneration (53–56). Our previous work (6), along with our new data on transgenic and viral induction of Yap5SA expression in the inner ear, provide clear evidence for Hippo as a major repressor of regeneration in the tissue, and explain why ablation of p27^{Kip1} is not sufficient to substantially relieve the block on supporting cell proliferation (9, 10).

Although constitutive activation of Yap clearly does not represent a therapeutically relevant strategy for augmenting proliferative regeneration in the sensory epithelia, locally administered small-molecule inhibition of the Hippo and p27^{Kip1} pathways may represent a viable strategy for mammalian hair cell regeneration.

Materials and Methods

Animal Care and Strains. All experiments were conducted in accordance with the policies of the Institutional Animal Care and Use Committees of Keck Medicine of USC and the Baylor College of Medicine. *p27*^{Kip1}*-GFP* mice were previously described in our laboratory (8). *Yap*$^{fl/fl}$ mice were described previously (34). *Sox2-CreER* and *Sox2-GFP* mice were obtained from The Jackson Laboratory. *Pax2-Cre* mice (33) were provided by Dr. Groves, Baylor College of Medicine. *Yap5SA* mice were described previously (35) and were kindly provided by Dr. Martin, Baylor College of Medicine.

Immunohistochemistry and EdU Labeling. Inner ears were identified, and cochleae or utricles were dissected and immunolabeled as described previously (6, 57). In brief, utricles and cochlear ducts were fixed in 4% formaldehyde for 20 min at room temperature (RT). Whole inner ears were fixed overnight (ON) at 4 °C, incubated in 30% sucrose ON at 4 °C, embedded in Tissue-Tek OCT (Sakura), and frozen in liquid-nitrogen vapor (6). Whole-mount sensory organs or 10-μm frozen sections were then blocked for 1 h to ON at RT in a blocking solution composed of 5% normal donkey serum (Sigma-Aldrich), 0.5% Triton X-100 (Sigma-Aldrich), and 20 mM Tris-buffered saline (10× TBS; Bio-Rad) at pH 7.5. Primary antibodies—goat anti-Sox2 (Santa Cruz Biotechnology and R&D Systems), mouse anti-p27^{Kip1} (Thermo Fisher Scientific), rabbit anti-Myo7A (Proteus Bioscience), rabbit anti-GFP (Torrey Pines Biolabs), rabbit anti-Ki67 (Abcam), active caspase 3 (R&D Systems), goat anti-Flag (Novus Biologicals), mouse anti-Yap (Santa Cruz Biotechnology), and rabbit anti-Yap (Cell Signaling Technology)—were reconstituted in blocking solution and applied overnight at 4 °C (6). Samples were washed with 20 mM TBS supplemented with 0.1% Tween 20 (Sigma-Aldrich), after which Alexa Fluor–labeled secondary antibodies (Life Technologies) were applied in the same solution supplemented with 3 μm DAPI (Sigma-Aldrich) for 2 h at RT.

EdU pulse-chase experiments were described previously (6) and initiated by a single i.p. injection of EdU (Abcam) at 50 ng per gram of body mass. Animals were euthanized at the indicated times, and the cells in the sensory epithelia were analyzed by Click-iT EdU labeling (Life Technologies).

Western Blot Analysis. The epithelial preparations of the cochlear ducts were isolated at E12.5 and E14.5 in ice-cold HBSS (Life Technologies) supplemented with a mixture of phosphatase/protease inhibitors (Cell Signaling Technology). The preparations were then lysed in 50 μL of RIPA lysis buffer (Cell

Signaling Technology) supplemented with the same mixture of protease inhibitors for 30 min at 4 °C. The BCA assay (Thermo Fisher Scientific) was used to determine the total protein concentration in each sample. Lysates were stored at −80 °C or used immediately for the subsequent analysis. Proteins were resolved on a NuPAGE 12% Bis-Tris Protein Gel (Thermo Fisher Scientific), transferred to a nitrocellulose membrane (Bio-Rad), and stained with an appropriate antibody, as described previously (6). The primary antibodies—rabbit anti-Yap (Cell Signaling Technology), rabbit anti-pYap (Ser127; Cell Signaling Technology), rabbit anti-Lats1 (Cell Signaling Technology), rabbit anti-pLats1 (Ser909; Cell Signaling Technology Technology), rabbit anti-Mst1 (Cell Signaling Technology), and rabbit anti-H3 (EMD Millipore)—were reconstituted at 1:10,000 in Odyssey blocking buffer (LI-COR), and the membranes were incubated ON at 4 °C. The membranes were washed in TBS supplemented with 0.1% Tween 20 (TBST) five times at RT. The anti-rabbit IR800 dye (LI-COR) was applied in TBST for 1 to 2 h at RT, and the membranes were imaged with an Odyssey CLx imaging system (LI-COR).

Adenoviral Gene Transfer. The pAnc80L65AAP vector (37) (Addgene plasmid 92307) was used to create adeno-associated viral vectors containing the full-length coding sequence of GFP or Yap5SA-GFP fusion protein (Addgene plasmid 33093) under the control of a cytomegalovirus promoter. Viral particles were packaged in HEK 293T cells and purified by CsCl-gradient centrifugation, followed by dialysis (Viral Vector Core Facility, Sanford Burnham Prebys Medical Research Institute). At P7, each animal was injected with 5 μL of virus at a titer of 10^{12} PFU/mL into the lateral ventricle as described previously for infection of central nervous system neurons (38).

RNA-Seq Analysis. Total RNA from FACS-purified organ of Corti progenitor cells was extracted using the Quick-RNA MicroPrep Kit (Zymo Research) and stored for up to 2 wk at −80 °C. RNA samples were then processed for library preparation with the QIAseq FX Single Cell RNA Library Kit (Qiagen), and the quality of the library was confirmed by Quick Biology using a Bioanalyzer. Two biological replicates were collected for each stage (E12.0 and E13.5), and at least 20 million 150-bp paired-end reads were sequenced for each replicate. The reads were mapped to the GRCm38/mm10 genome assembly using STAR (58). Differentially expressed protein coding genes were identified by DESeq2 (FDR <0.05) (59). For data visualization, principal component analysis was performed by PCAExplorer using the top 1,000 most significantly differentially expressed genes (60).

ATAC-Seq and CUT&RUN. The ATAC-seq protocol was described previously (61). Tn5 transposase was expressed and purified according to Picelli et al. (62) and used with the following modifications. In brief, 5,000 FACS-purified progenitor cells were used for each of three biological replicates sequenced for E12.0 and E13.5 organ of Corti. Tn5 transposition was performed for 20 min at 37 °C. At least 30 million paired-end reads were sequenced for each sample.

The CUT&RUN method for in situ ChIP, described previously (19, 20), was used to profile Tead occupancy and lysine 27 acetylation on histone 3 (H3K27Ac) of the chromatin in E12.0 and E13.5 progenitors. At least 20,000 cells were used for each of two Tead CUT&RUNs, 5,000 cells were used for each of two biological replicates of H3K27Ac for E12.0 and E13.5 progenitor cells, and 1,000 cells were used as IgG-only control. Protein A/MNase fusion protein was a kind gift from Dr. Steven Henikoff's laboratory, Fred Hutchinson Cancer Research Center. Rb anti-pan Tead (Cell Signaling Technology) and rb anti-H3K27Ac (Active Motif) antibodies were used. To construct CUT&RUN libraries, Accel-NGS 2S plus DNA prep kits with single index and molecular identifiers (Swift Bioscience) were used. At least 20 million paired-end reads were sequenced for each sample.

Encode pipelines were adapted for alignment and quality control for ATAC-seq and CUT&RUN data. In brief, the next-generation reads were trimmed to 37 bp and aligned to the GRCm38/mm10 genome assembly (58). PCR duplicates were removed based on genomic coordinates for ATAC-seq, or by molecular identifiers using UMI-tools for CUT&RUN (63). Peaks were called by model-based analysis of ChIP-Seq (MACS2) with a FDR <0.01 and the dynamic lambda (–nolambda) option for individual replicates (64). IDR or pooled peaks were identified between the biological replicates for each sample and used for the downstream analysis. bigWig files were generated with deepTools (65). Individual genomic loci were visualized with the Integrative Genomics Viewer (IGV) (66) using fold-enrichment tracks generated in MACS2 (64, 67). Heatmaps were generated with deepTools based on normalized bigWig signal files. To identify transcription factor binding enrichment in the subsets of the genomic regions, the whole genome was used as a background in HOMER (18).

Data Availability. All sequencing data for RNA, ATAC, and CUT&RUN analysis have been deposited in the National Center for Biotechnology Information's Gene Expression Omnibus (GEO) database, accession number GSE149254.

ACKNOWLEDGMENTS. We thank Francis James for his contributions to constructing the pipelines for the RNA-seq, ATAC-seq, and CUT&RUN data analysis and quality control; Dr. Rickard Sandberg for providing pTXB1-Tn5 plasmid and the protocols for Tn5 transposase purification; Haoze Vincent Yu for optimizing this protocol; and Dr. Steven Henikoff for providing the A/MNase fusion protein. This work was supported by grants to K.G. from the National Institute on Deafness and Other Communication Disorders (NIDCD) (R21DC016984); to T.T. from the NIDCD (F31DC017376); to J.F.M. from the NIH (HL127717, HL130804, and HL118761), Vivian L. Smith Foundation, State of Texas funding, and Fondation LeDucq Transatlantic Networks of Excellence in Cardiovascular Research (14CVD01); to M.W. from the NIDCD (R01DC006283); to A.K.G. from the NIDCD (DC014832); and to N.S. from the Hearing Restoration Program of the Hearing Health Foundation and from the NIDCD (R01DC015829). K.G. and M.B were also supported by training grants (T32DC009975 and T32DC000022, respectively) from the NIDCD.

1. D. K. Wu, M. W. Kelley, Molecular mechanisms of inner ear development. *Cold Spring Harb. Perspect. Biol.* **4**, a008409 (2012).
2. R. J. Ruben, Development of the inner ear of the mouse: A radioautographic study of terminal mitoses. *Acta Otolaryngol.* (suppl. 220):220, 1–44 (1967).
3. X. Yang *et al.*, Establishment of planar cell polarity is coupled to regional cell cycle exit and cell differentiation in the mouse utricle. *Sci. Rep.* **7**, 43021 (2017).
4. J. C. Burns, D. On, W. Baker, M. S. Collado, J. T. Corwin, Over half the hair cells in the mouse utricle first appear after birth, with significant numbers originating from early postnatal mitotic production in peripheral and striolar growth zones. *J. Assoc. Res. Otolaryngol.* **13**, 609–627 (2012).
5. K. Gnedeva, A. J. Hudspeth, SoxC transcription factors are essential for the development of the inner ear. *Proc. Natl. Acad. Sci. U.S.A.* **112**, 14066–14071 (2015).
6. K. Gnedeva, A. Jacobo, J. D. Salvi, A. A. Petelski, A. J. Hudspeth, Elastic force restricts growth of the murine utricle. *eLife* **6**, e25681 (2017).
7. P. Chen, N. Segil, p27(Kip1) links cell proliferation to morphogenesis in the developing organ of Corti. *Development* **126**, 1581–1590 (1999).
8. Y.-S. Lee, F. Liu, N. Segil, A morphogenetic wave of p27Kip1 transcription directs cell cycle exit during organ of Corti development. *Development* **133**, 2817–2826 (2006).
9. H. Löwenheim *et al.*, Gene disruption of p27(Kip1) allows cell proliferation in the postnatal and adult organ of Corti. *Proc. Natl. Acad. Sci. U.S.A.* **96**, 4084–4088 (1999).
10. H. Laine, M. Sulg, A. Kirjavainen, U. Pirvola, Cell cycle regulation in the inner ear sensory epithelia: Role of cyclin D1 and cyclin-dependent kinase inhibitors. *Dev. Biol.* **337**, 134–146 (2010).
11. Z. Meng, T. Moroishi, K.-L. Guan, Mechanisms of Hippo pathway regulation. *Genes Dev.* **30**, 1–17 (2016).
12. B. Zhao *et al.*, TEAD mediates YAP-dependent gene induction and growth control. *Genes Dev.* **22**, 1962–1971 (2008).
13. L. M. Koontz *et al.*, The Hippo effector Yorkie controls normal tissue growth by antagonizing scalloped-mediated default repression. *Dev. Cell* **25**, 388–401 (2013).
14. H. Oh *et al.*, Genome-wide association of Yorkie with chromatin and chromatin-remodeling complexes. *Cell Rep.* **3**, 309–318 (2013).
15. G. G. Galli *et al.*, YAP drives growth by controlling transcriptional pause release from dynamic enhancers. *Mol. Cell* **60**, 328–337 (2015).
16. F. Zanconato *et al.*, Genome-wide association between YAP/TAZ/TEAD and AP-1 at enhancers drives oncogenic growth. *Nat. Cell Biol.* **17**, 1218–1227 (2015).
17. K. Arnold *et al.*, Sox2(+) adult stem and progenitor cells are important for tissue regeneration and survival of mice. *Cell Stem Cell* **9**, 317–329 (2011).
18. S. Heinz *et al.*, Simple combinations of lineage-determining transcription factors prime cis-regulatory elements required for macrophage and B cell identities. *Mol. Cell* **38**, 576–589 (2010).
19. P. J. Skene, S. Henikoff, An efficient targeted nuclease strategy for high-resolution mapping of DNA binding sites. *eLife* **6**, e21856 (2017).
20. P. J. Skene, J. G. Henikoff, S. Henikoff, Targeted in situ genome-wide profiling with high efficiency for low cell numbers. *Nat. Protoc.* **13**, 1006–1019 (2018).
21. M. P. Creyghton *et al.*, Histone H3K27ac separates active from poised enhancers and predicts developmental state. *Proc. Natl. Acad. Sci. U.S.A.* **107**, 21931–21936 (2010).
22. A. Rada-Iglesias *et al.*, A unique chromatin signature uncovers early developmental enhancers in humans. *Nature* **470**, 279–283 (2011).
23. C. Y. McLean *et al.*, GREAT improves functional interpretation of cis-regulatory regions. *Nat. Biotechnol.* **28**, 495–501 (2010).
24. S. L. Prescott *et al.*, Enhancer divergence and cis-regulatory evolution in the human and chimp neural crest. *Cell* **163**, 68–83 (2015).
25. M.-C. Lai, W.-C. Chang, S.-Y. Shieh, W.-Y. Tarn, DDX3 regulates cell growth through translational control of cyclin E1. *Mol. Cell. Biol.* **30**, 5444–5453 (2010).

26. H. Fang *et al*., RecQL4-Aurora B kinase axis is essential for cellular proliferation, cell cycle progression, and mitotic integrity. *Oncogenesis* **7**, 68 (2018).
27. C. J. Sherr, D-type cyclins. *Trends Biochem. Sci.* **20**, 187–190 (1995).
28. A. W. Hunter *et al*., The kinesin-related protein MCAK is a microtubule depolymerase that forms an ATP-hydrolyzing complex at microtubule ends. *Mol. Cell* **11**, 445–457 (2003).
29. A. Subramanian *et al*., Gene set enrichment analysis: A knowledge-based approach for interpreting genome-wide expression profiles. *Proc. Natl. Acad. Sci. U.S.A.* **102**, 15545–15550 (2005).
30. J. Kwan *et al*., DLG5 connects cell polarity and Hippo signaling protein networks by linking PAR-1 with MST1/2. *Genes Dev.* **30**, 2696–2709 (2016).
31. I. M. Moya, G. Halder, Hippo-YAP/TAZ signalling in organ regeneration and regenerative medicine. *Nat. Rev. Mol. Cell Biol.* **20**, 211–226 (2019).
32. B. C. Cox *et al*., Spontaneous hair cell regeneration in the neonatal mouse cochlea in vivo. *Development* **141**, 816–829 (2014).
33. T. Ohyama, A. K. Groves, Generation of Pax2-Cre mice by modification of a Pax2 bacterial artificial chromosome. *Genesis* **38**, 195–199 (2004).
34. N. Zhang *et al*., The Merlin/NF2 tumor suppressor functions through the YAP oncoprotein to regulate tissue homeostasis in mammals. *Dev. Cell* **19**, 27–38 (2010).
35. T. O. Monroe *et al*., YAP partially reprograms chromatin accessibility to directly induce adult cardiogenesis in vivo. *Dev. Cell* **48**, 765–779.e7 (2019).
36. B. I. Carlborg, J. C. Farmer Jr., Transmission of cerebrospinal fluid pressure via the cochlear aqueduct and endolymphatic sac. *Am. J. Otolaryngol.* **4**, 273–282 (1983).
37. L. D. Landegger *et al*., A synthetic AAV vector enables safe and efficient gene transfer to the mammalian inner ear. *Nat. Biotechnol.* **35**, 280–284 (2017).
38. J.-Y. Kim, S. D. Grunke, Y. Levites, T. E. Golde, J. L. Jankowsky, Intracerebroventricular viral injection of the neonatal mouse brain for persistent and widespread neuronal transduction. *J. Vis. Exp.*, 51863 (2014).
39. J. S. Golub *et al*., Hair cell replacement in adult mouse utricles after targeted ablation of hair cells with diphtheria toxin. *J. Neurosci.* **32**, 15093–15105 (2012).
40. V. Munnamalai, D. M. Fekete, Wnt signaling during cochlear development. *Semin. Cell Dev. Biol.* **24**, 480–489 (2013).
41. B. E. Jacques *et al*., A dual function for canonical Wnt/β-catenin signaling in the developing mammalian cochlea. *Development* **139**, 4395–4404 (2012).
42. R. Chai *et al*., Wnt signaling induces proliferation of sensory precursors in the postnatal mouse cochlea. *Proc. Natl. Acad. Sci. U.S.A.* **109**, 8167–8172 (2012).
43. F. Shi, L. Hu, A. S. B. Edge, Generation of hair cells in neonatal mice by β-catenin overexpression in Lgr5-positive cochlear progenitors. *Proc. Natl. Acad. Sci. U.S.A.* **110**, 13851–13856 (2013).
44. W. Ni *et al*., Extensive supporting cell proliferation and mitotic hair cell generation by in vivo genetic reprogramming in the neonatal mouse cochlea. *J. Neurosci.* **36**, 8734–8745 (2016).
45. L. Jansson *et al*., β-Catenin is required for radial cell patterning and identity in the developing mouse cochlea. *Proc. Natl. Acad. Sci. U.S.A.* **116**, 21054–21060 (2019).
46. F. Yao *et al*., SKP2- and OTUD1-regulated non-proteolytic ubiquitination of YAP promotes YAP nuclear localization and activity. *Nat. Commun.* **9**, 2269 (2018).
47. T. Cardozo, M. Pagano, The SCF ubiquitin ligase: Insights into a molecular machine. *Nat. Rev. Mol. Cell Biol.* **5**, 739–751 (2004).
48. W. Jang, T. Kim, J. S. Koo, S.-K. Kim, D.-S. Lim, Mechanical cue-induced YAP instructs Skp2-dependent cell cycle exit and oncogenic signaling. *EMBO J.* **36**, 2510–2528 (2017).
49. J. T. Corwin, D. A. Cotanche, Regeneration of sensory hair cells after acoustic trauma. *Science* **240**, 1772–1774 (1988).
50. B. M. Ryals, E. W. Rubel, Hair cell regeneration after acoustic trauma in adult Coturnix quail. *Science* **240**, 1774–1776 (1988).
51. P. Weisleder, E. W. Rubel, Hair cell regeneration after streptomycin toxicity in the avian vestibular epithelium. *J. Comp. Neurol.* **331**, 97–110 (1993).
52. J. S. Stone, E. W. Rubel, Cellular studies of auditory hair cell regeneration in birds. *Proc. Natl. Acad. Sci. U.S.A.* **97**, 11714–11721 (2000).
53. X. Varelas *et al*., The Hippo pathway regulates Wnt/beta-catenin signaling. *Dev. Cell* **18**, 579–591 (2010).
54. T. Heallen *et al*., Hippo pathway inhibits Wnt signaling to restrain cardiomyocyte proliferation and heart size. *Science* **332**, 458–461 (2011).
55. M. Imajo, K. Miyatake, A. Iimura, A. Miyamoto, E. Nishida, A molecular mechanism that links Hippo signalling to the inhibition of Wnt/β-catenin signalling. *EMBO J.* **31**, 1109–1122 (2012).
56. B. R. Kuo, E. M. Baldwin, W. S. Layman, M. M. Taketo, J. Zuo, In vivo cochlear hair cell generation and survival by coactivation of β-catenin and Atoh1. *J. Neurosci.* **35**, 10786–10798 (2015).
57. K. Gnedeva, A. J. Hudspeth, N. Segil, Three-dimensional organotypic cultures of vestibular and auditory sensory organs. *J. Vis. Exp.*, 10.3791/57527 (2018).
58. A. Dobin *et al*., STAR: Ultrafast universal RNA-seq aligner. *Bioinformatics* **29**, 15–21 (2013).
59. M. I. Love, W. Huber, S. Anders, Moderated estimation of fold change and dispersion for RNA-seq data with DESeq2. *Genome Biol.* **15**, 550 (2014).
60. F. Marini, H. Binder, pcaExplorer: An R/Bioconductor package for interacting with RNA-seq principal components. *BMC Bioinformatics* **20**, 331 (2019).
61. J. D. Buenrostro, P. G. Giresi, L. C. Zaba, H. Y. Chang, W. J. Greenleaf, Transposition of native chromatin for fast and sensitive epigenomic profiling of open chromatin, DNA-binding proteins and nucleosome position. *Nat. Methods* **10**, 1213–1218 (2013).
62. S. Picelli *et al*., Tn5 transposase and tagmentation procedures for massively scaled sequencing projects. *Genome Res.* **24**, 2033–2040 (2014).
63. T. Smith, A. Heger, I. Sudbery, UMI-tools: Modeling sequencing errors in unique molecular identifiers to improve quantification accuracy. *Genome Res.* **27**, 491–499 (2017).
64. J. Feng, T. Liu, B. Qin, Y. Zhang, X. S. Liu, Identifying ChIP-seq enrichment using MACS. *Nat. Protoc.* **7**, 1728–1740 (2012).
65. F. Ramírez, F. Dündar, S. Diehl, B. A. Grüning, T. Manke, deepTools: a flexible platform for exploring deep-sequencing data. *Nucleic Acids Res.* **42**, W187–W191 (2014).
66. H. Thorvaldsdóttir, J. T. Robinson, J. P. Mesirov, Integrative genomics Viewer (IGV): High-performance genomics data visualization and exploration. *Brief. Bioinform.* **14**, 178–192 (2013).
67. Y. Zhang *et al*., Model-based analysis of ChIP-seq (MACS). *Genome Biol.* **9**, R137 (2008).